A Planar-Coil-Based Current Transducer Used in Distribution Power System

Peng Wang, Guixin Zhang, and Zheng Qian

***Abstract*—For measuring currents flowing in three-phase rectangular-shaped busbars, in this paper, a planar coil with air core is used as a current sensing unit. The vector potential of the busbar and the electromotive forces of the planar coil for single- and three-phase currents are calculated with a numerical integration arithmetic. The relative error caused by adjacent busbars was simulated when the transducers were used for the three-phase current measurement. The simulation results show that the relative error induced by the adjacent busbars is less than 2%. Planar-coil-based current transducers enclosed with silicon rubber insulator are developed. The successful field trial of the transducers for more than four years shows that the transducers can meet the field requirement.**

***Index Terms*—Busbar, current measurement, fault currents, high-voltage (HV) techniques, magnetic transducer, magnetic vector potential, planar coil.**

I. Introduction

RECTANGULAR busbars are commonly used in many electrical power distribution equipment, such as high-voltage (HV) switchgear cabinet at medium HV level (10 or 35 kV). In modern distribution power systems, the fault current through such equipment can reach up to 50–100 kA. Due to the magnetic saturation phenomena, the conventional current transformers possess quite poor dynamic range and could not accurately measure such a heavy fault current.

The planar coils mentioned in the references are widely used in current measurements at low voltage [1]–[4]. They are usually constructed on printed circuit boards and surround current-carrying conductor. Therefore, they are seemly not suitable for the measurement of currents in three-phase busbar at higher voltage level.

In this paper, a noncontact current transducer, based on a planar coil and enclosed with strong silicon rubber insulator, was developed for this purpose. Unlike conventional current transformers and the Rogowski coils, the suggested transducers do not need to enclose the conductors. Hence, it can easily be installed above the busbars.

Manuscript received October 25, 2009; revised January 11, 2010; accepted January 13, 2010. Date of publication April 19, 2010; date of current version October 13, 2010. This work was supported by the Natural Science Foundation of China under Contract 50707001. The Associate Editor coordinating the review process for this paper was Dr. Subhas Mukhopadhyay.

P. Wang and G. Zhang are with the State Key Laboratory of Power System, Department of Electrical Engineering, Tsinghua University, Beijing 100084, China (e-mail: wpeng@tsinghua.edu.cn; guixin@tsinghua.edu.cn).

Z. Qian is with the School of Instrument Science and Optoelectronics Engineering, BeiHang University, Beijing 100083, China (e-mail: qianzheng@buaa.edu.cn).

Color versions of one or more of the figures in this paper are available online at http://ieeexplore.ieee.org.

Digital Object Identifier 10.1109/TIM.2010.2046600

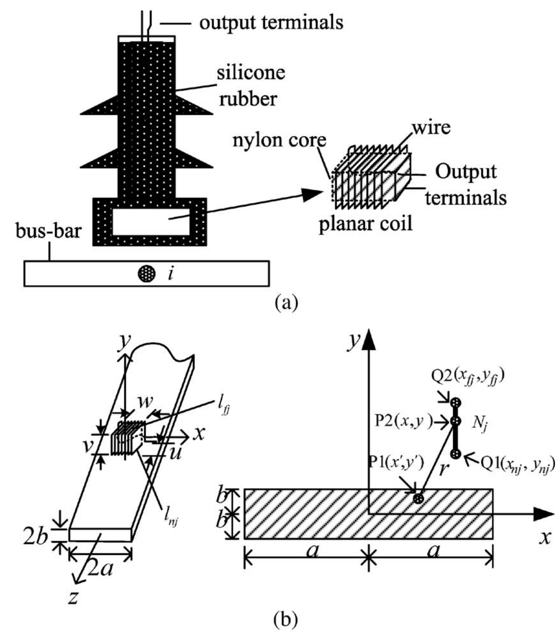

Fig. 1. Structure of (a) the planar-coil-based transducer and the planar coil and (b) the planar coil parameters and the rectangular section of the busbar.

The operation principle of the planar coil is presented in the first part of Section II; then, the design of the insulation structure of the transducer follows. In Section III, the experiment results of the transducer are shown, and its field trial in a substation is given in Section IV. This paper concludes in Section V.

II. Principle of Operation

A. Principle of Operation for the Transducer

The transducer is based on measuring the magnetic field at a small area near the surface of the conductor. Because the magnetic field intensity at a specific point outside the conductor has a certain relationship with the current, the current can be obtained through the output of the planar coil placed near the conductor. The planar coil is inserted into a silicon rubber insulator shown in Fig. 1.

The planar coil is a solenoid with length w, width u, height v, and turn number N, as shown in Fig. 1. The planar coil has a nylon core of rectangular cross section; the busbar has a rectangular cross section with sides of length $2a$ and width $2b$. The transducer is placed as such so that the width side of the planar coil is parallel to the direction of the current.

It is set that the current i flowing through the busbar is along the positive z-direction. The magnetic field intensity $\mathbf{B}$

surrounding the busbar can be deduced using the following equation:

$$\mathbf{B} = \nabla \times \mathbf{A} \tag{1}$$

where $\mathbf{A}$ is the magnetic vector potential outside the conductor.

Consequently, the magnetic flux through the jth turn of the coil is

$$\varphi_j = \iint_s \mathbf{B} \cdot d\mathbf{s} = \iint_s (\nabla \times \mathbf{A}) \cdot d\mathbf{s} \tag{2}$$

where s is the coil cross-sectional area, and the normal of s is perpendicular to the current i and along the positive x-direction. Upon invoking Stokes' theorem into (2), we can get

$$\varphi_j = \oint_l \mathbf{A} \cdot d\mathbf{l} \tag{3}$$

where l is the contour of the jth turn of the planar coil. As previously depicted, the planar coil has a rectangular shape, with two of its four segments being perpendicular to the current flowing through the busbar, so only the other two parallel segments contribute to the dot product in (3) because the magnetic vector potential A is in the same direction as the current i, as the current is along just one direction, as shown in Fig. 1(b). With regard to the two parallel segments of the jth turn of the planar coil, we denote the segment adjacent to the busbar as l_{nj}, and the other as l_{fj}, as shown in the left side of Fig. 1(b).

In Fig. 1(b), we choose the normal of each turn of the planar coil along the positive x-direction so that the direction chosen for l_{nj} is in the negative z-direction and l_{fj} is in the positive z-direction according to right-hand rule. Consequently, (3) can be transformed to

$$\varphi_j = \mathbf{A}_{fj} \cdot \mathbf{l}_{fj} + \mathbf{A}_{nj} \cdot \mathbf{l}_{nj} = (A_{fj} - A_{nj}) u \cos\alpha \tag{4}$$

where α is the angle between the current flowing direction and the direction of vector l_{fj} (supposed that the normal of the jth turn is parallel to the surface of the conductor). With the descriptions given, α is equal to 0. The positions of l_{fj} and l_{nj} are shown in the left side of Fig. 1(b).

The field of a current distributed over the cross section of a conductor can be found by integrating the fields of an infinite number of line currents that can be deemed to constitute the distributed current. Because the axial z-component of the vector potential of a line current is [5]

$$A = \frac{\mu_0}{2\pi} i \log r \tag{5}$$

where r is the distance from the conductor to the point at which $\mathbf{A}$ exists, the total magnetic vector potential at a specific point outside the conductor can be obtained by integrating (5) over the section of the conductor.

In Fig. 1(b), point $\mathrm{P1}(x', y')$ is inside the busbar, point $\mathrm{P2}(x, y)$ is outside the busbar, r is the distance between P1 and P2, point $\mathrm{Q1}(x_{nj}, y_{nj})$ is on l_{nj}, and point $\mathrm{Q2}(x_{fj}, y_{fj})$ is on l_{fj}.

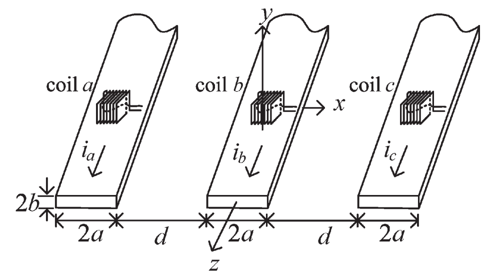

Fig. 2. Structure of the transducer and the planar coil.

The frequency of the busbar current considered in this paper is as low as 50 Hz, so the eddy current effects are weak. For simplicity, when neglecting the eddy currents, for current i flowing in the busbar, the current density is $i/4ab$, and the current i carried by a filament of cross section $dx'dy'$, where x' and y' are coordinates of any filament in the busbar, is $(i/4ab)\ dx'dy'$. The field of all the elements of the busbar is given by substituting for i in (5) and integrating over the section of the rectangle [5].

In Fig. 1(b), supposed that L is the length of the busbar. When $L \gg r$, the axial z-component of the vector potential at point $\mathrm{P2}(x, y)$ with distance r from $\mathrm{P1}(x', y')$ is

$$A = \frac{\mu_0 i}{16\pi ab} \iint_D \ln\left[(x - x')^2 + (y - y')^2\right] dx'dy' \tag{6}$$

where $D = \{(x', y') | -a \le x' \le a, -b \le y' \le b\}$.

The magnetic flux through the turn of the planar coil is equal to the closed-loop line integration of the vector potential $\mathbf{A}$ near the turn of the coil. Upon substituting (3), the expression for the electromotive force for the jth turn of the planar coil is

$$e_j = -\frac{d\varphi_j}{dt}. \tag{7}$$

Use of (4) and (6) in (7) gives

$$\begin{aligned} e &= \sum_{j=1}^{N} e_j = -\sum_{j=1}^{N} \frac{d\varphi_j}{dt} \\ &= -\sum_{j=1}^{N} \frac{\mu_0 u \cos\alpha}{16\pi ab} \frac{di}{dt} \\ &\quad \times \iint_D \ln \frac{((x_{fj} - x')^2 + (y_{fj} - y')^2)}{((x_{nj} - x')^2 + (y_{nj} - y')^2)} dx'dy' \end{aligned} \tag{8}$$

where N is the total turn numbers of the coil, i is the current flowing through the conductor, and μ_0 is the permeability in vacuum. Based on the coil parameters and the relative position between the coil and the busbar, x_{nj}, x_{fj}, y_{nj}, and y_{fj} are known. The value of e can be calculated using (8).

When the three-phase currents are measured with the planar coils, the result can be affected by the nearby phase currents. For example, in Fig. 2, i_b and i_c may contribute to the voltage output of the coil a.

In Fig. 2, the electromotive force of coil a consists of e_{aa} (contributed by i_a), e_{ba} (contributed by i_b), and e_{ca} (contributed by i_c); they are respectively generated by the three-phase current. Using (8) gives

$$\begin{aligned} e_{aa} &= \sum_{j=1}^{N} e_{aaj} \\ &= \sum_{j=1}^{N} \Bigg(-\frac{\mu_0 u \cos\alpha}{16\pi ab} \frac{di_a}{dt} \\ &\qquad \times \iint\limits_{D_{aa}} \ln \frac{(x_{fj}-x')^2+(y_{fj}-y')^2}{(x_{nj}-x')^2+(y_{nj}-y')^2} dx'dy' \Bigg) \end{aligned} \tag{9}$$

where $D_{aa}=\{(x',y')|-(3a+d)\leq x'\leq -(a+d), -b\leq y'\leq b\}$, and where d is the spacing between two conductors, as shown in Fig. 2. We also have

$$\begin{aligned} e_{ba} &= \sum_{j=1}^{N} e_{baj} \\ &= \sum_{j=1}^{N} \Bigg(-\frac{\mu_0 u \cos\alpha}{16\pi ab} \frac{di_b}{dt} \\ &\qquad \times \iint\limits_{D_{ba}} \ln \frac{(x_{fj}-x')^2+(y_{fj}-y')^2}{(x_{nj}-x')^2+(y_{n_j}-y')^2} dx'dy' \Bigg) \end{aligned} \tag{10}$$

where $D_{ba} = \{(x',y')| -a \leq x' \leq a, -b \leq y' \leq b\}$, and

$$\begin{aligned} e_{ca} &= \sum_{j=1}^{N} e_{caj} \\ &= \sum_{j=1}^{N} \Bigg(-\frac{\mu_0 u \cos\alpha}{16\pi ab} \frac{di_c}{dt} \\ &\qquad \times \iint\limits_{D_{ca}} \ln \frac{(x_{fj}-x')^2+(y_{fj}-y')^2}{(x_{nj}-x')^2+(y_{nj}-y')^2} dx'dy' \Bigg) \end{aligned} \tag{11}$$

where $D_{ca} = \{(x',y')|a+d \leq x' \leq 3a+d, -b \leq y' \leq b\}$.

Therefore, the total electromotive force of the planar coil a is

$$e_a = e_{aa} + e_{ba} + e_{ca}. \tag{12}$$

In (12), e_{ba} and e_{ca} can be taken as the influence with regard to e_{aa}. Taking this into account, the uncertainty of the planar coil a in the measurement values of current i_a in Fig. 2 is

$$\varepsilon\% = \frac{E_{a-aa}}{E_a} \times 100 \tag{13}$$

where E_{a-aa} and E_a are the RMS values of $(e_a - e_{aa})$ and e_a.

The output of coil b with e_{ab}, e_{bb}, and e_{cb}, and coil c with e_{ac}, e_{bc}, and e_{cc}, can be obtained by using the same method in deducing the expressions given by (9)–(11).

B. Insulation Structure of the Transducer

The software package Ansoft SB is used to simulate the potential and electric field intensity distribution inside the transducer. For the convenience of simulation, it is suggested that the transducer is placed above a grounded metal plane, and an HV of 42 kV is applied to the output terminals [the terminals are shown in Fig. 1(a)]. The simulated results are shown in Fig. 3.

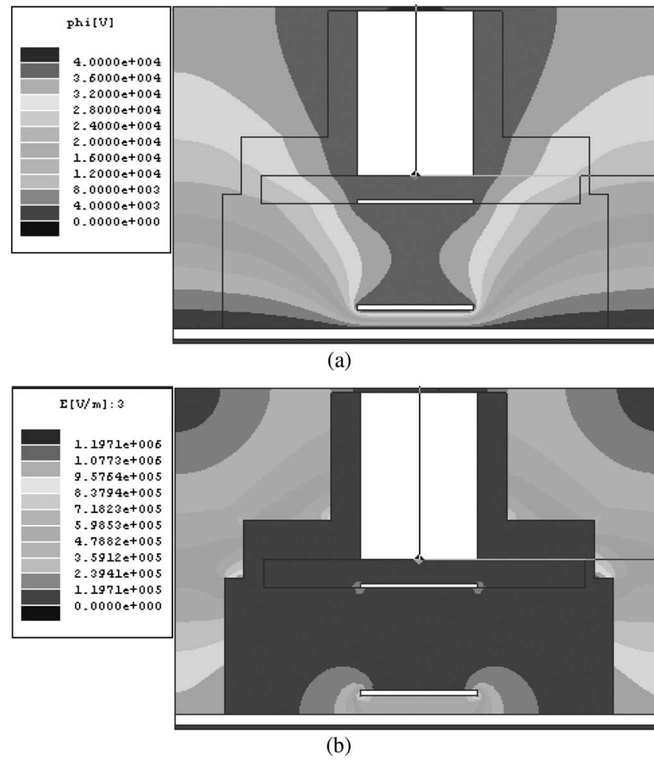

Fig. 3. (a) Electric potential distribution and (b) electric field intensity distribution inside the transducer.

According to related standard of China, the equipment and devices working at 10-kV voltage must withstand a test voltage of 42 kV in 5 min. When an HV of 42 kV is applied to the transducer, the electric potential distribution inside the transducer is shown in Fig. 3(a). Fig. 3(b) reveals that the maximum electric field intensity appears at the bottom corners of the coil inside the transducer. Therefore, in these places, a thicker insulation should be added and the corners should be more smoothed. The final maximum electric field intensity inside the transducer is less than 1.2×10^6 V/m, which is far less than the withstand electric field of the silicone rubber.

III. Design and Performance Evaluation

A. Structure Parameters of the Planar Coil and Accuracy Calibration

The planar coil is of a rectangular cross section with sides of length 20 × 20 mm, and its length w is equal to 25 mm; the busbar also has a rectangular cross section with sides of length 80 mm and 8 mm, and its length is 500 mm. The coil has 154 turns of copper wire (with diameter of 0.16 mm).

The planar coil is placed in the middle position of the rectangular busbar, and the distance from the axis of the coil to the top side of the busbar is 13.5 mm. Current is applied through a current source with the range of 1–600 A. The calibration setup for the coil is shown in Fig. 4. The outputs of the standard current transformer and the coil are measured with an Agilent 34410A digit multimeter. The experimental and theoretical data are listed in Fig. 5.

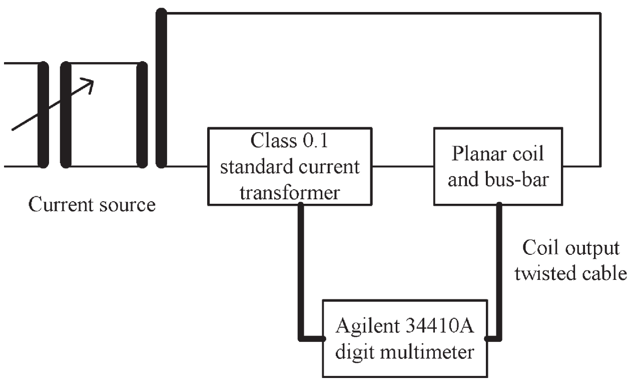

Fig. 4. Output characteristic test circuit for the planar coil.

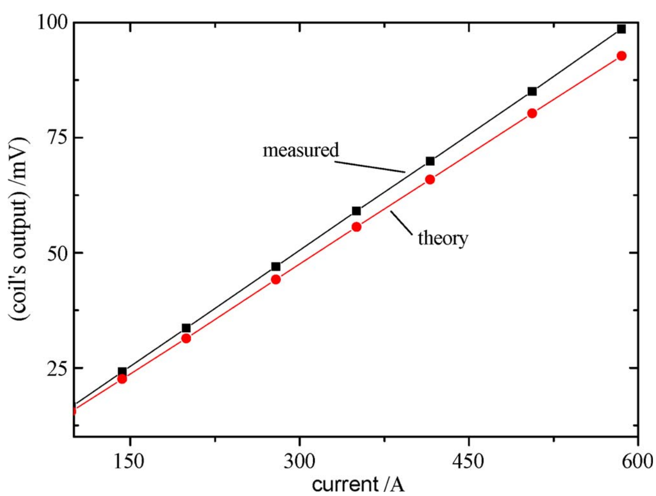

Fig. 5. Relationship between the current through the busbar and the voltage output of the coil.

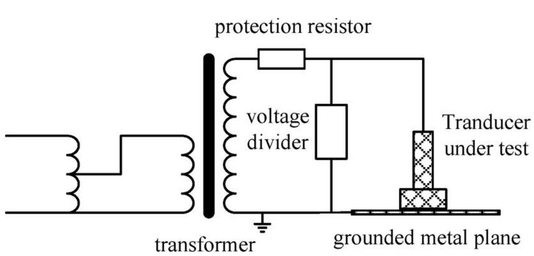

Fig. 6. Circuit diagram for the withstand voltage test.

In Fig. 5, the theory curve is obtained using (8) with the parameters previously given. In the figure, the theoretical calculation has some similarity with the measured results. The differences between them can be explained by considering the test setup during the accuracy test because the length of the busbar is about 0.5m long, except for this busbar current, and the remaining part of the primary current loop may contribute to the output of the coil. Hence, the measured values are larger than the theoretical values in Fig. 5.

B. HV Withstand Test

As previously stated, the transducers are working at 10-kV voltage level. It is required to withstand 42-kV HV of 50 Hz within 5 min. During the voltage withstand test, the HV is applied to the output terminals of the transducer, and a grounded metal plane is placed under it, as shown in Fig. 6.

TABLE I
ADDITIONAL ERROR UNDER THE INFLUENCE OF ADJACENT CURRENTS

Coil	E_x(mV)	E_{xx}(mV)	$E_{x\text{-}xx}$(mV)	Additional error (%)
Coil a	83.41	84.25	1.34	1.61
Coil b	83.50	84.25	0.75	0.90
Coil c	83.41	84.25	1.34	1.61

TABLE II
UNCERTAINTY BUDGETS DURING THE CALIBRATION

Components	Magnitude
Standard current transformer	0.1%
Agilent 34410A multimeter	0.1%
Position between coil and busbar	1.5%

A voltage divider is used for the measurement of the voltage applied to the transducer under test. The test results show that all of the transducers can pass the 42-kV voltage withstand test without any flashover or breakdown.

C. Relative Error Under the Influence of Adjacent Busbars

The transducer's output depends on the busbar current and its relative position to the busbar. The relative errors due to misalignment were reported in [6]. When the horizontal misalignment between the transducer and busbar is less than 5 mm, the relative error is less than about 1.5% [6].

The influence of nearby busbars to the transducers in field operation should be considered, and it will produce an additional error.

In field applications, the busbar has a cross section with sides of length 80 mm and 8 mm, and the spacing between two adjacent busbars d shown in Fig. 2 is equal to 130 mm. Supposed that the three-phase current is

$$\begin{cases} i_a = I_0 \cos(\omega t - 120^\circ) \\ i_b = I_0 \cos \omega t \\ i_c = I_0 \cos(\omega t + 120^\circ) \end{cases} \tag{14}$$

where $\omega = 2\pi f$, and $f = 50$ Hz.

In view of (9)–(11), and (14), we can get the output of each of the three-phase coils due to the contribution of the other two adjacent busbars. When the amplitude I_0 of the current is 500 A, the additional error of coil a due to the influence of i_b and i_c, and that for coil b due to i_a and i_c, and that for coil c due to i_a and i_b, are listed in Table I.

In Table I, the subscript x in E_x, E_{xx}, and E_{x-xx} denotes the coil a, b and c, respectively.

From Table I, we can conclude that the additional error caused by adjacent currents is less than 2%. It is accurate enough for the accuracy requirement to the transducers (less than 5% in amplitude).

The uncertainty budgets during the calibration are shown in Table II.

From Table II, we can conclude that the amplitude uncertainty in the calibration is less than 1.8%.

IV. FIELD TRIAL

In field installation, three transducers constitute a group, which is used to measure the three-phase busbar currents inside

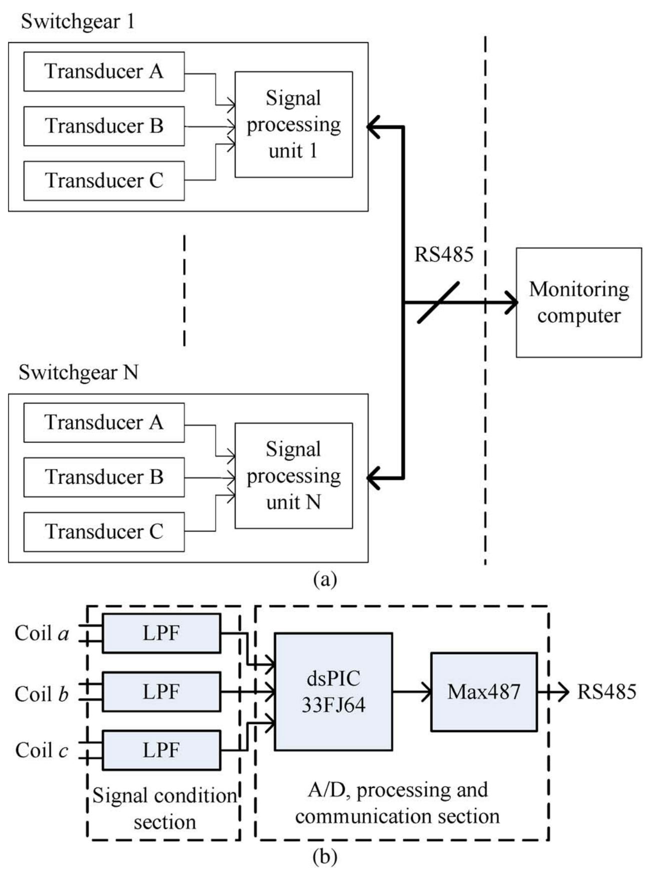

Fig. 7. (a) Structure diagram of the measuring system. (b) Simplified block diagram for the signal processing unit. LPF: low-pass filter.

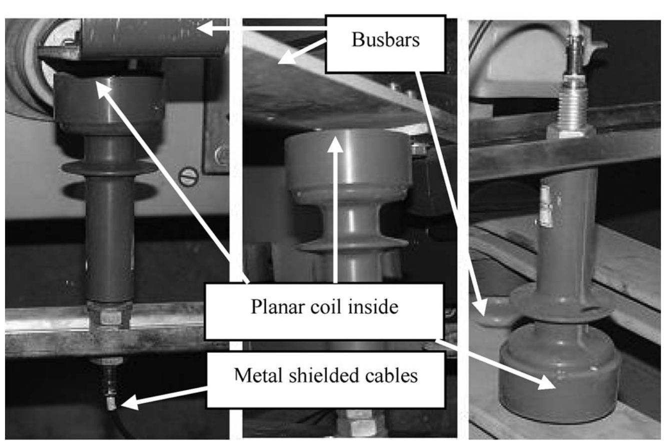

Fig. 8. Photos of current transducer installation.

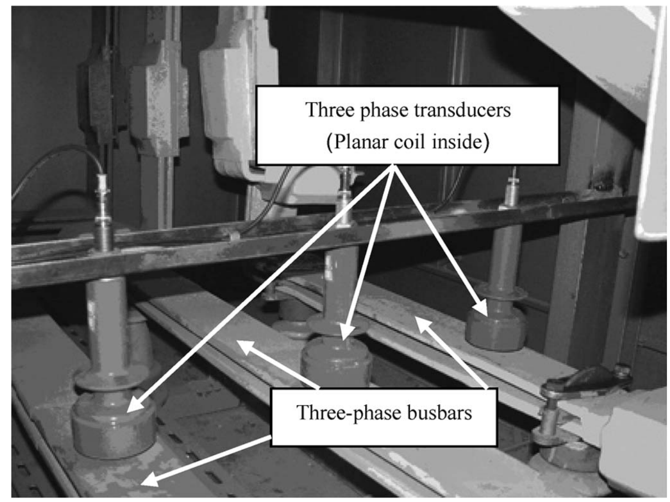

Fig. 9. Structure diagram for sensing part installation.

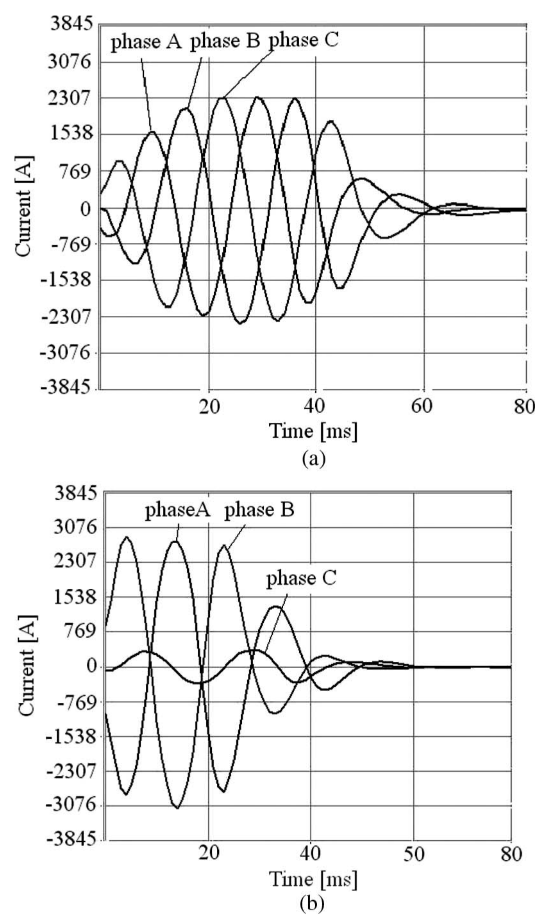

Fig. 10. Fault current waveforms under field trial. (a) Three-phase fault. (b) Fault between phases A and B.

the switchgear cabinet. The output signals of the transducers are transmitted through a metal shielded cable with a length of 2 m to a microcontroller-based signal processing unit encapsulated inside a shielded box. All outputs of the signal processing units are connected to a PC with an RS485 bus. The diagram structure of the measuring system is shown in Fig. 7.

In Fig. 7(a), each of the switchgear cabinets $1 \sim N$ contains three transducers and one signal processing unit. They are used to measure and process the three-phase currents inside the cabinet. The signal processing unit mainly consists of a microcontrolled unit (MCU), and its simplified architecture is shown in Fig. 7(b).

A photo of the current transducer installation is shown in Fig. 8.

About 60 transducers were installed in a substation in the City of Xinxiang, Henan Province, China. One of the installation structures is shown in Fig. 9.

During the field trial for more than four years, the current transducers have shown good performance and measured several types of fault currents. Two types of fault current waveforms are plotted in Fig. 10.

The rated currents flowing through the three-phase busbars are less than 1000 A; in some cases, it is even as less as 50–80 A. In Fig. 10, the maximum currents measured by the transducers during the fault condition are over 2300 A.

V. Conclusion

The design of a unique current transducer for the measurement of fault currents in the HV switchgear cabinet has been presented. The transducer has a planar coil and a silicon rubber enclosure. These transducers can easily be installed inside already existing switchgear cabinet. The simulation results show that the relative errors induced by the adjacent busbars are less than 2%.

Compared with similar applications using planar coils in the references, this paper has first reported that a planar-coil-based current transducer is used to measure short circuit current in switchgear cabinet. The transducers possess nonmagnetic saturation and a large dynamic range. The result of field trial reveals that they are suitable for applications in heavy fault current measurement.

References

[1] C. Dudek, F. Duverger, M. Ledieu, S. Dubourg, and O. Acher, "A new type of highly compact planar inductor," *IEEE Trans. Magn.*, vol. 43, no. 6, pp. 2621–2623, Jun. 2007.

[2] S. Brugger and O. Paul, "Field-concentrator-based resonant magnetic sensor with integrated planar coils," *J. Microelectromech. Syst.*, vol. 18, no. 6, pp. 1432–1443, Dec. 2009.

[3] J. T. Conway, "Noncoaxial inductance calculations without the vector potential for axisymmetric coils and planar coils," *IEEE Trans. Magn.*, vol. 44, no. 4, pp. 453–462, Apr. 2008.

[4] Y. P. Su, X. Liu, and S. Y. R. Hui, "Mutual inductance calculation of movable planar coils on parallel surfaces," *IEEE Trans. Power Electron.*, vol. 24, no. 4, pp. 1115–1124, Apr. 2009.

[5] K. J. Fields, P. J. Lawrenson, and C. W. Trowbridge, *The Analytical and Numerical Solution of Electric and Magnetic Fields*. New York: Wiley, 1992.

[6] P. Wang, G. Zhang, X. Zhu, and C. Luo, "Planar Rogowski coil current transducer used for three-phase plate-form busbars," in *Proc. IEEE Instrum. Meas. Technol. Conf.*, Warsaw, Poland, 2007, pp. 1–4.

Peng Wang was born in Henan, China, in 1977. He received the Ph.D. degree in electrical engineering from Tsinghua University, Beijing, China, in 2006.

He is currently an Assistant Researcher with the Department of Electrical Engineering, Tsinghua University. His research interests include high-voltage electronic instrument transformers, high-frequency transducers that are used under ultrahigh-voltage environment and power electronics, calibration instrumentation for electronic instrument transformers, and all-digital power metering systems that are used in high-voltage power systems.

Guixin Zhang was born in China, on April 14, 1963. He received the B.S. and M.S. degrees from Tsinghua University, Beijing, China, in 1987, and 1993, respectively, and the Ph.D. degree from Nanyang Technological University, Singapore, in 1999.

He is currently an Associate Professor with the Department of Electrical Engineering, Tsinghua University. His research interests include high-voltage engineering, optical fiber sensors, and plasma.

Zheng Qian was born in Zhengzhou, China, in 1973. He received the Ph.D. degree in electrical engineering from Xi'an Jiaotong University, Xi'an, China, in 2000.

He was a Postdoctoral Fellow with Tsinghua University, Beijing, China. Since 2002, he has been a Professor of instrument science and technology with BeiHang University, Beijing. His research interests include advanced sensor technology, high voltage test, online monitoring and fault diagnosis of power equipment, etc.